Int J Adv Manuf Technol (2007) 33: 7–17
DOI 10.1007/s00170-006-0453-2

ORIGINAL ARTICLE

A. Ameli · M. R. Movahhedy

# A parametric study on residual stresses and forging load in cold radial forging process

Received: 2 August 2005 / Accepted: 7 February 2006 / Published online: 30 March 2006


**Abstract** In this work, a comprehensive study of radial forging process is presented through 2-D axisymmetric and 3-D finite element simulations while considering internal tube profile. The tube used in this investigation has four internal helical grooves along its length. The material is modeled with the elastic-plastic behavior, and sliding-sticking friction model is utilized to model the die-workpiece and mandrel-workpiece contacts. The numerical results in the 2-D case are compared with available experimental data. Residual stresses in the forged product, stress concentration around the grooves, pressure distribution on the hammers and mandrel and maximum forging load are studied. The effects of process parameters such as workpiece and die geometries, percentage of deformation, and workpiece motions on residual stresses and applied pressures on the hammers and mandrel are investigated. The results provide a valuable insight into the parameters affecting radially forged products and provide a useful tool for better design of this process.

**Keywords** Finite element · Profiled tubes · Radial forging · Residual stress

## 1 Introduction

Radial forging is a cost-effective and material-saving forming process for reducing the round, square and rectangle cross-sections of rods, tubes, and shafts. This process may be performed in cold or hot state on metals such as steel alloys, titanium alloys, beryllium, tungsten, and high-temperature super-alloys [1]. Further, it is used for producing axially stepped shafts and internally profiled tubes such as helically grooved tubes, which are the focus of this work. Such products normally operate under dynamic loading conditions. Therefore, prediction and control of residual stresses and stress concentration for enhancing the fatigue life and dimensional stability of such products is essential. In addition, due to the high cost of mandrels used in this process for forging of hard materials, forecasting the applied pressures on the mandrel and optimizing its life is important. The most popular usages of this process are listed bellow [1–3]:

- Forging of railroad axles and turbine shafts,
- Producing tubes with and without internal profiles,
- Reducing of ingots made from special alloys when low volumes does not justify a rolling mill,
- Forging of preforms prior to the finish forging of large turbine blades,
- Production of large diameter -up to1,000 mm-seamless tubing for energy applications,
- Rifling of gun barrels (hot and cold).

Radial forging process has the capability for virtually chipless manufacturing of rods and tubes to provide a precision-finished product with almost 95% material utilization [2]. The properties of products of radial forging include tight tolerances, smooth surface finish, preferred fiber structure, minimum notch effect, and homogenous grains due to full penetration of deformation to the core of the workpiece. [1, 3, 4]. The process properties include high efficiency in energy consumption, often considerable material savings, avoiding surface cracks, center bursts, and suck-in at the ends of workpiece, and short process cycle time.

In the radial forging process, the workpiece is usually manipulated between two horizontal chuck-heads which clamp and position the workpiece. The forging box consists of two or four radially reciprocating hammer dies with polar layouts. The dies are actuated by connecting rods driven by electric motor shafts rotating at a speed between 200 to 1,000 rpm depending on the machine size [3]. Deformation, in the process results from a large

A. Ameli · M. R. Movahhedy (✉)
School of Mechanical Engineering,
Sharif University of Technology,
P.O. Box 11365-9466,
Azadi Ave.,
Tehran, Iran
e-mail: movahhed@sharif.edu
Tel.: +98-21-66165505
Fax: +98-21-66000021

number of short-stroke and high-speed hammer blows on the workpiece. After each blow, the workpiece is rotationally indexed and axially fed toward the entrance of dies. Consequently, at each stroke only a small portion of the workpiece is subjected to plastic deformation, thereby a fairly low deformation load is required.

The simultaneous rotational motion and axial feed of the workpiece allows for production of round pieces and internally-profiled tubes. When an internal profile is required, an idly rotating mandrel with inverted profile is placed inside the tube. Forging the tube around this mandrel will create the required internal profile. A schematic view of the radial forging process is given in Fig. 1.

Figure 2 shows the deformation zones in radial forging. Deformation in this process occurs in three distinctive zones: the sinking zone, the forging zone, and the sizing zones. In the sinking zone, both inner and outer diameters of the tube are reduced. In the forging zone, inner diameter of the tube is equal to the outer diameter of mandrel and only the outer diameter of the tube is reduced. Finally, in the sizing zone, both inner and outer diameters of the tube have almost reached their final sizes and only a small amount of plastic deformation occurs in the tube.

In the past, several studies on the radial forging process have appeared in the literature. In 1976, Lahoti and Altan obtained distribution of stresses in the sinking, forging, and sizing zones using the slab method analysis [5]. They also investigated the design of dies with compound-angles for radial forging of rods and tubes [2, 6]. Paukert investigated the flow of material during radial forging process [7]. Rodic et al. studied the basic concepts of finite element modeling of radial forging process [8]. Later, Jackman et al. analyzed radial forging process as a quasi-steady-state analysis and predicted the distribution of temperature and strain using finite element [9, 10]. Shivpuri and Domblesky simulated radialy forging of Pyromet 18 and concluded that the deformation is uniform during the process [11–13]. They developed and validated multiple pass radial forging of large diameter tubes. Altan et al. reviewed technology of the radial forging process for design of preform [14]. Jang and Liou investigated residual stresses in symmetric products by nonlinear finite element [4]. Subramanian et al. modeled the die cavity filling in radial forging of rifling by upper-bound method [15].

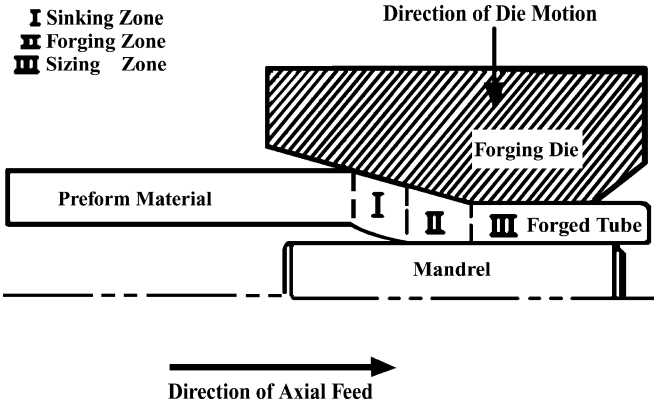


**Fig. 2** Deformation zones (sinking, forging and sizing) in radial forging process

For most radial forging products, prediction and control of residual stresses is essential for enhancing their fatigue life and dimensional stability. Since experiments that are used to determine the residual stresses and required deformation loads are generally expensive and time consuming, a numerical simulation might be used to investigate the various aspects of radial forging process.

Previous analytical and numerical studies on this process are mostly limited to 2D-axisymmetric models for simple products or have not considered internal profiles. In this work, both a2D-axisymmetric and 3-D models of the radial forging process are presented. In particular, radial forging of tubes with internal profiles is considered. The tube used in this investigation has four internal helical grooves along its length. The axisymmetric simulation of radial forging is used to study the effects of process parameters on residual stress distributions and on the die pressure. The main purpose of this study is to investigate material flow during filling of internal grooves, the pattern of residual stresses in forged product and the stress concentration around the grooves that are vital to the fatigue life of the product. The effects of geometric parameters such as tube preform inner diameter and thickness and the percentage of deformation on residual stresses and applied normal pressures to the

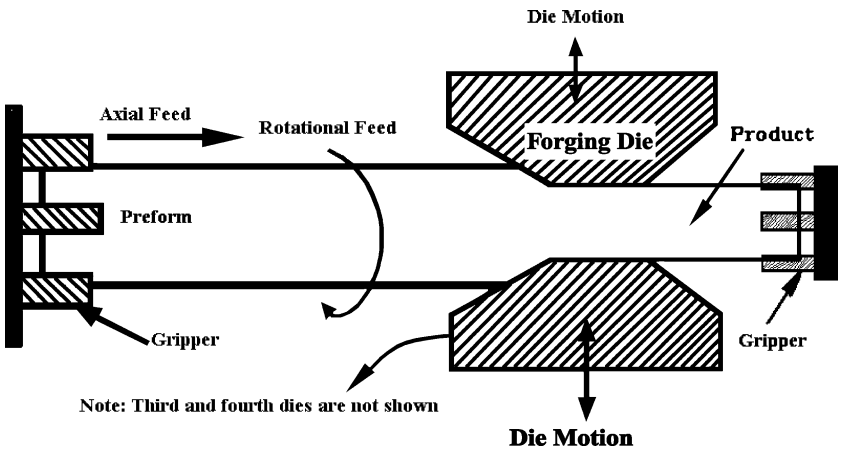


**Fig. 1** A general schematic view of radial forging process

**Table 1** Various types of elements used in models

| Part | Element Type in 2D | Element Type in 3D |
|---|---|---|
| **Tube** | **CAX4R**<br>4 Nodes Continuum Rectangular Element with Reduced Integration | **C3D8R**<br>8 Nodes Continuum Cube Element with Reduced Integration |
| **Die and Mandrel** | **RAX2**<br>2 Nodes Rigid Line Element | **R3D4**<br>4 Nodes Rigid Rectangular Element |

mandrel are investigated. Furthermore, the effect of workpiece rotational feed on residual stresses in outer surface and normal pressure on the dies and mandrel are studied through 3-D simulation, because these effects cannot be seen in an axisymmetric model. The material is modeled with elastic-plastic behavior, and the sliding-sticking friction model and penalty method are used to model the die-workpiece and mandrel-workpiece contact surfaces in both axisymmetric and 3-D models.

## 2 Formulation

In this simulation, the elastic-plastic deformation of material is assumed to be associated with the boundary value problem where the stress and strain field solutions satisfy the equilibrium equations, the constitutive equation, and the prescribed boundary values. The workpiece is assumed to obey the Von–Misses yield criterion and its associated flow rule. The weak form of the equilibrium equation, neglecting body force, is expressed as:

$$\int_v \sigma_{ij,j}\,\delta v_i dV = 0, \tag{1}$$

where $\sigma_{i,j}$ is the component of stress tensor, $\delta\nu_i$ is an arbitrary variation of velocity, and comma denotes partial differentiation. Using the divergence theorem, and the symmetry of the stress tensor, imposing the essential boundary condition $\delta_v$=0 on $S_v$, where $S_v$ is the specified velocity field boundary, and decomposing the stress tensors into the deviatoric $\sigma'_{ij}$ and hydrostatic $\sigma_m$ components, Eq. 1 becomes:

$$\int_v \sigma'_{ij}\delta\dot{\varepsilon}_{ij}dV + \int_v \sigma_m\delta\dot{\varepsilon}_v dV - \int_{S_F} T_i\delta v_i dS = 0, \tag{2}$$

where $\dot{\varepsilon}_{ij}$ is the strain-rate and $\dot{\varepsilon}_v$ is the volumetric strain-rate. The final equation can be obtained by replacing the related terms with the effective stress and the effective strain-rate in the first integral. The incompressibility constraint on the admissible velocity field in Eq. 2 can be removed by a penalty function constant, K, as follows:

$$\delta\pi = \int_v \overline{\sigma}\delta\dot{\overline{\varepsilon}}dV + K\int_v \dot{\varepsilon}_v dV - \int_{S_F} T_i\delta v_i dS = 0, \tag{3}$$

where $\overline{\sigma} = \sqrt{(3/2)\sigma'_{ij}\sigma'_{ij}}$, $\dot{\overline{\varepsilon}} = \sqrt{(2/3)\dot{\varepsilon}_{ij}\dot{\varepsilon}_{ij}}$ and $K$ is a large positive constant. Equation 3 is the final form of the basic equation for the finite element discretization.

**Table 2** Elastic-plastic properties of material

| | |
|---|---|
| Elasticity modulus | 203 GPa |
| Poisson's ratio | 0.29 |
| Initial yield stress | 200 MPa |
| K | 750 MPa |
| n | 0.2 |

## 3 Modeling

In the present work, the ABAQUS commercial FE code is used for simulation of radial forging process [16]. 8-node cube continuum elements and 4-node rectangular continuum elements with reduced integration formulations are used for modeling the workpiece and 4-node rigid and 2-node rigid elements are used for modeling the die and mandrel rigid surfaces in axisymmetric and 3-D simulations, respectively. Table 1 summarizes these data.

Since the process is assumed to be cold forging, a power law for strain hardening is used ($\sigma$=$K\varepsilon^n$) and the effects of strain rate and temperature are neglected because the heat generated in the process, is not high enough to change material or process parameters significantly and thus, the process maybe assumed as isothermal. In other words, it may be argued the heat generation during plastic deformation offsets the heat dissipation by cooling. The elastic-plastic properties for workpiece material are given in Table 2.

Die-workpiece and mandrel-workpiece contact is modeled using the rigid-deformable finite sliding contact

**Table 3** Mandrel-workpiece and die-workpiece contacts properties

| | |
|---|---|
| Sliding type | Small sliding |
| Formulation | Penalty |
| Master surface | Rigid in 2D<br>Rigid rectangle in 3D |
| Slave surface | Solid edge in 2D<br>Solid surface in 3D |

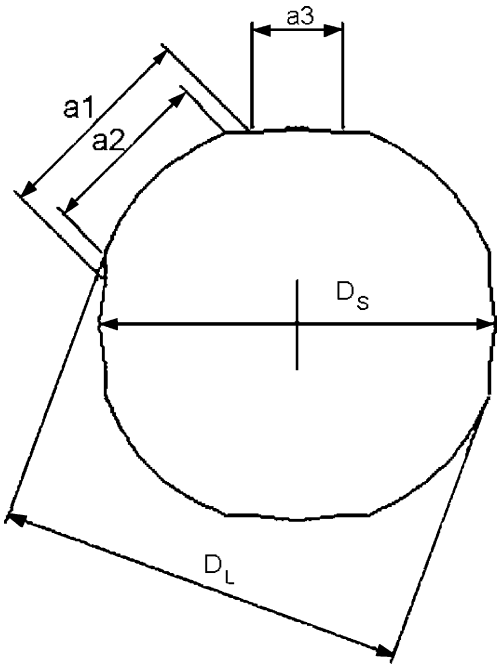


**Fig. 3** Cross-section of mandrel with helical grooves

model. Penalty formulation is utilized to model contact in both axisymmetric and 3-D simulations. A sliding-sticking friction model is imposed as contact behavior; frictional stress obeys the Coulomb law when this stress is less than shear yield stress of workpiece material. Otherwise, the friction model shifts to sticking state $\tau = m\sigma_y/\sqrt{3}$ where $m$ is the frictional coefficient and $\sigma_y$ is the normal yield stress of workpiece material [17, 18]. Properties of mandrel-workpiece and die-workpiece contacts are summarized in Table 3.

In the 2-D axisymmetric simulation, the non-symmetric features of the process such as internal profile and small gaps between hammers at the end of blowing are neglected and an axisymmetric distribution of residual stresses on the inner and outer surfaces of the workpiece is assumed. This

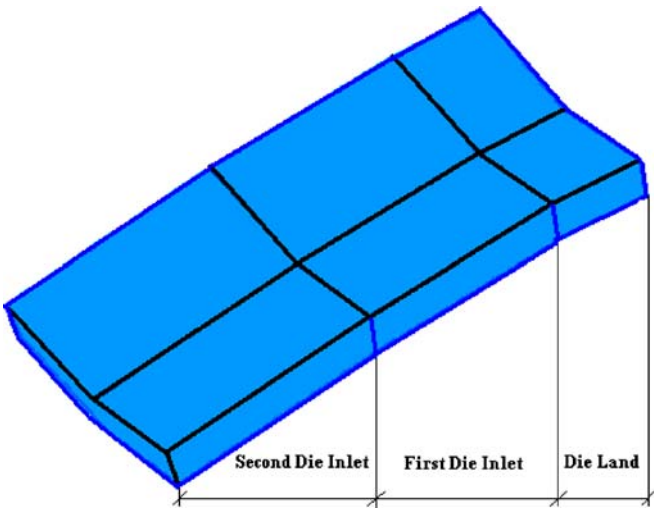


**Fig. 4** Die land and die inlets of hammer in radial forging process

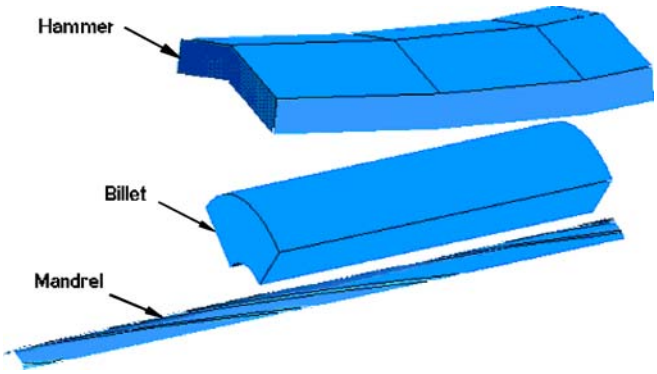


**Fig. 5** Components layout in 3-D simulation of radial forging process

simplification is necessary for increasing the efficiency and speed computation and its results are useful for qualitative investigation of parameters such as axial feed per stroke, friction, die land length, and die inlet angles which may get limited effects from the presence of internal profile. Therefore, the distribution of residual stresses in the inner and outer surfaces of workpiece and applied pressure on the hammers and variation of these parameters with respect to the axial feed per stroke of tube, friction between die-tube and mandrel-tube, and geometry of die are studied through the axisymmetric model. Subsequently, a 3-D simulation is used for more thorough investigation of the process and the effect of the presence of the internal profile on process parameters.

Figure 3 shows the geometry of the mandrel used in the 3-D simulation. The cross-section shown is used for producing desired profiled tube. The change in the diameter of the mandrel ($D_L$ and $D_S$) is for creating four grooves with a depth of $((D_L - D_S)/2)$. This grooved section is swept helically along the axial direction of mandrel with a helix angle of 5° 47′. The effects of these helical grooves on the residual stresses in the inner surface

**Table 4** Geometry of the workpiece, hammer, and mandrel used in modeling of radial forging process

| | |
|---|---|
| | Geometry of the tube |
| Outer radius of preform | 15.5 mm |
| Inner radius of preform | 5.8 mm |
| Outer radius of product | 12 mm |
| Inner radius of product | 3.915 mm |
| Percentage of reduction | 37% |
| | Geometry of the hammer |
| Die land length | 10 mm |
| 1st die inlet angle | 6° |
| 2nd die inlet angle | 9.5° |
| 1st die inlet length | 21 mm |
| 2nd die inlet length | 24 mm |
| Total length of die | 70 mm |
| | Geometry of the mandrel |
| Large diameter ($D_L$) | 7.965 mm |
| Small diameter ($D_S$) | 7.685 mm |

**Table 5** Comparisons between loads from FE, slab method and experiment in the radial forging process

| Sample No. | Billet Dia. | Product Dia. | Load By FE (KN) | Load By Exp.(KN) [19] | Load by Slab (KN) [2] |
|---|---|---|---|---|---|
| 1 | 15.97 | 13.18 | 177.4 | 172.00 | 171.98 |
| 2 | 15.97 | 13.25 | 174.6 | 167.00 | 170.62 |
| 3 | 15.03 | 13.11 | 137.2 | 124.00 | 143.37 |
| 4 | 13.99 | 13.03 | 65.1 | 74.00 | 106.18 |
| Ave. | | | 138.57 | 134.25 | 148.03 |

of forged tube and applied pressure on the mandrel surface are investigated in this work. Figure 4 shows the geometry of the hammers used in this study. This hammer has a die land and two die inlets with different angles.

Because of the periodic symmetry in the process geometry only a quarter (or 1/8 in some cases) of the workpiece and mandrel with a complete hammer are utilized in modeling. The layout of modeled components is shown in Fig. 5 and the geometric data for workpiece, hammers and mandrel is presented in Table 4.

The grippers that hold the workpiece can apply front-pull or back-push forces to reduce the forging load. The effects of the front-pull and back-push on the workpiece ends are modeled by imposing pressure boundary condition at the ends. Both the die and the mandrel are modeled as rigid bodies and so, each of them have a reference point that controls them. In other words, axial and radial displacements of the die and the mandrel are imposed using the reference points.

## 4 Validation of axisymmetric model

Before presenting the simulation results, it is necessary to investigate the validity of the numerical model. In the absence of direct experimental data, it is chosen to validate the results against some experimental data presented in the past literature for forging of cylindrical parts without internal profile. Therefore, the FE results obtained from the axisymmetric model is compared with both experimental [19] and slab method analysis results presented by Lahoti and Altan [2]. For this purpose, a finite element simulation of radial cold forging of AISI 1015 steel billet with a friction factor of 0.15, inlet angle of 4.3°, and axial feed per stroke of 0.37 mm is carried out. Table 5 lists the predicted loads from FE and slab method analysis, in comparison with results of experimental measurements. Agreement between the FE, slab method, and experiment is observed, especially in samples 1 and 2. Moreover better agreement between FE and experimental results is seen than between slab method and experimental results. Therefore, it can be deduced that the developed finite element model for radial forging is valid and more accurate than slab method. Consequently, the developed FE model can be used in evaluating and predicting of other aspects of radial forging process such as residual stresses and normal pressures.

## 5 Numerical results and discussion

In this section, the effects of various process parameters such as geometries, motions and friction on the residual stresses of product, normal pressures on die and mandrel, and required deformation load are investigated using axisymmetric and 3-D models of radial forging process.

### 5.1 Axisymmetric modeling

First, the results of axisymmetric modeling are presented. Distribution of residual stresses along the axial direction of workpiece and effects of axial feed per stroke and friction on the residual stress are discussed. In addition, the variation of the hammer pressure and maximum forging load due to process parameters such as thickness of the preform, die inlet angle, die land length and axial feed per stroke is investigated.

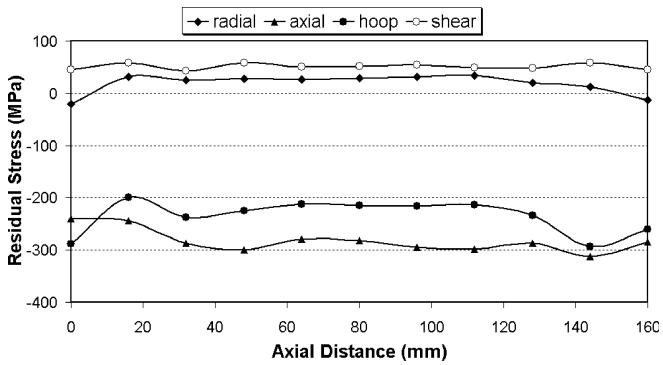


**Fig. 6** Distribution of axial, hoop, radial, and shear residual stresses on the inner surface along tube length

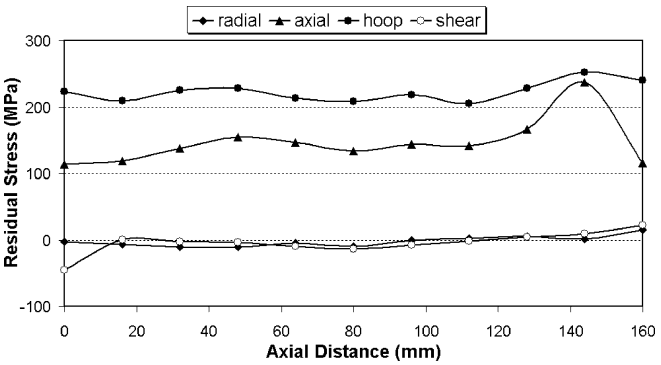


**Fig. 7** Distribution of axial, hoop, radial, and shear residual stresses on the outer surface along tube length

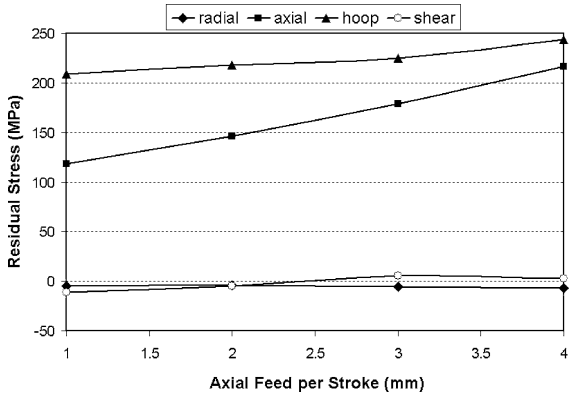


**Fig. 8** Variation of axial, hoop, radial, and shear residual stresses with the axial feed per stroke on the outer surface of the forged tube

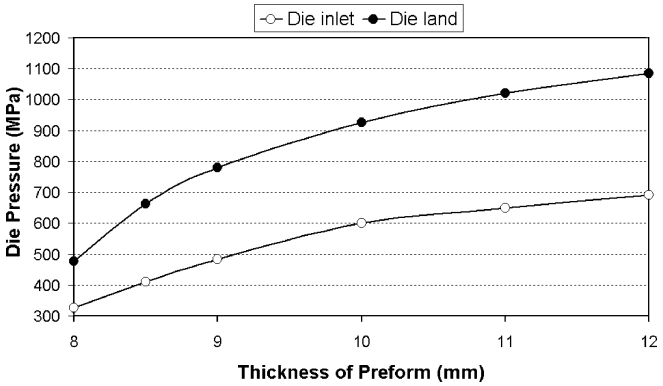


**Fig. 10** Variation of pressure on the die land and inlet zone with the thickness of preform

### *5.1.1 Residual stresses*

Figures 6 and 7 show the profile of radial, axial, hoop, and shear residual stresses along the axial direction on the inner and outer surfaces of the workpiece, respectively, for an axial feed of 2 mm/stroke. The distribution of all these stresses is almost uniform along the tube length except at its ends. In comparison with the axial and hoop stresses, radial and shear stresses on both the inner and outer surfaces are small and negligible. This is expected because once the hammers are removed; these surfaces are free and thus, the radial stress must vanish on them. Also, because of the symmetric nature of the process and the model, the residual shear stresses must be low. Indeed, the small but nonzero nodal stresses obtained from FE are generated because the stresses obtained at the integration points of the elements are averaged at nodal points on the surface.

The axial and hoop residual stresses on the inner surface are compressive and thus, can help in preventing the crack propagation. Since such products usually operate under high internal pressures, compressive residual stresses on the inner surface can enhance product life. On the other hand, the stresses on the outer surface are tensile and thus, may assist the propagation of possible cracks and might need to be stress released before use.

The variation of residual stresses on the outer surface vs. the axial feed per stroke of workpiece is shown in Fig. 8. It can be seen that the radial and shear stresses are low and do not change with increasing of the axial feed. However, the axial and hoop stresses increase almost linearly with an increase of the axial feed per stroke. Consequently, the larger stresses are affected significantly by variation of axial feed.

In Fig. 9, variations of residual stresses with the friction coefficients between the die-tube and mandrel-tube are presented. It was assumed that the friction coefficients between die-tube and mandrel-tube are equal and changes in a range of 0.025 to 0.150, because the process is cold forming. All stresses vary only slightly with friction coefficient.

### *5.1.2 Die pressure and forging load*

In this section, the effects of workpiece preform and die geometries on the die pressure and required forming load are investigated. To study the effects of the perform thickness, the final tube geometry and the inner radius of preform are held constant and only the outer radius, of preform is varied. Variation of average pressure on the die land and first die inlet with the thickness of workpiece

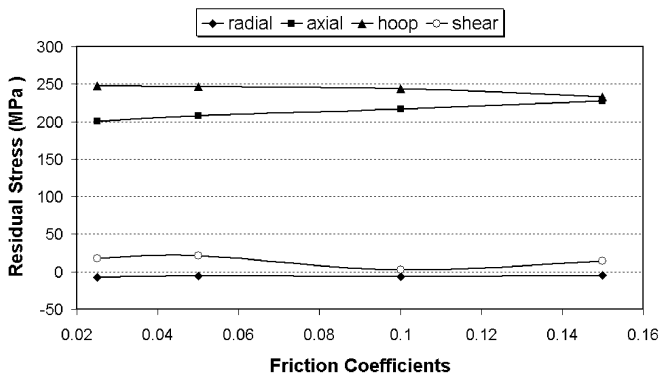


**Fig. 9** Variation of axial, hoop, radial, and shear residual stresses with friction coefficient between die-tube and mandrel-tube on the outer surface of the forged tube

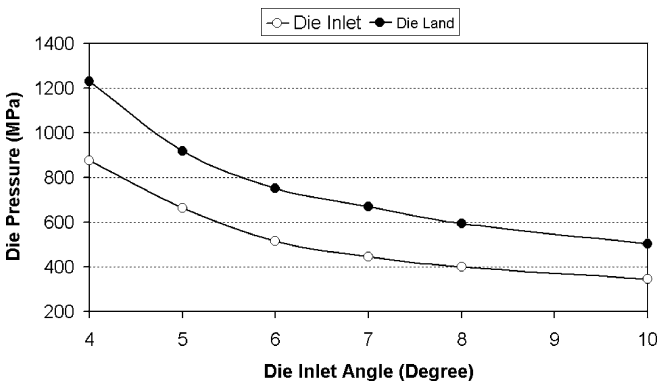


**Fig. 11** Variation of die pressure with die inlet angle

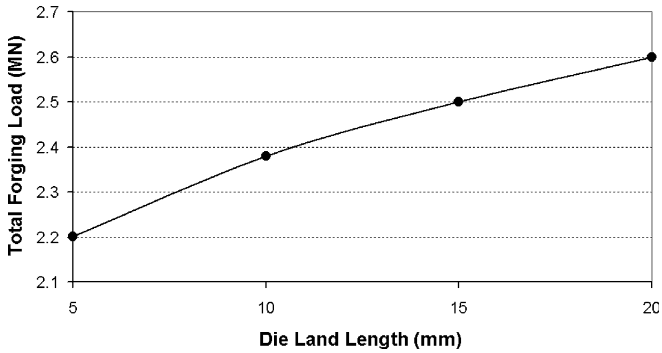


**Fig. 12** Variation of total forging load with die land length

preform is given in Fig. 10. The pressure on the die land is larger than die inlet pressure, and both the die inlet and die land pressures rise with increasing the workpiece preform thickness but die land pressure varies at a slightly higher rate. Therefore, because of its large value and higher sensitivity, the pressure at the die land seems to be more critical as the limiting factor for hammer life.

Next, the effect of die inlet angle on the die pressure is discussed. Figure 11 shows the variations of pressure on the die land and die inlet as the die inlet angle is increased. It is shown that larger die inlet angles create lower pressures at both the die land and die inlet such that the pressures are reduced by 50% when the die inlet angle rises from 4° to 10°. Consequently, increasing the die inlet angle might be used to improve die life.

Finally, the effects of the forging parameters on the maximum forging load are considered. To calculate the total forging load, the average pressure on the hammers is obtained from results and is multiplied by the contacting area of hammers at the end of the die stroke. Forging load variations with respect to the die land length, axial feed per stroke, and friction coefficients are depicted in Figs. 12, 13, and 14, respectively. The relationship between load and all these parameters is almost linear and total forging load increases with an increase in these parameters. It seems that friction coefficient has the largest effect on forging load and axial feed per stroke has the least effect. Therefore, it can be concluded that the axial feed per stroke affect the critical residual stresses severely while its effect on forging load is not significant, whereas the friction coefficient has the reverse effect. Consequently, for optimization of the process, these parameters must be suitably adjusted.

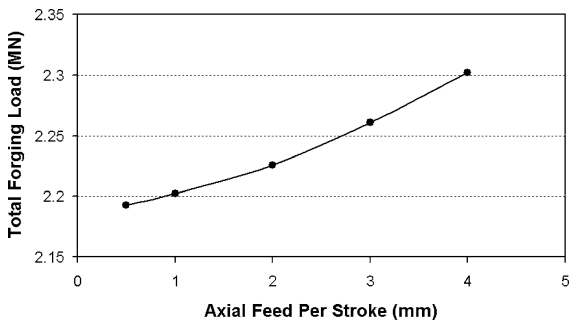


**Fig. 13** Variation of total forging load with axial feed per stroke

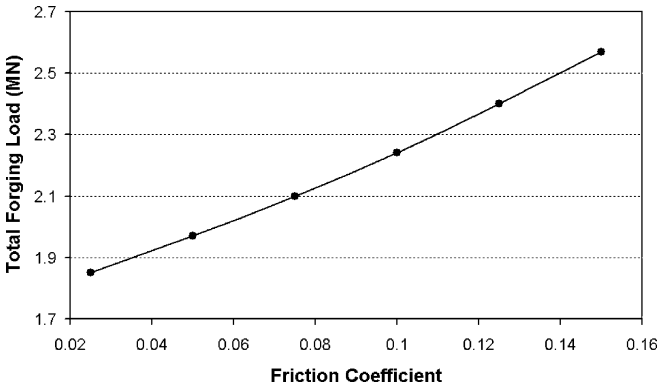


**Fig. 14** Variation of total forging load with friction coefficient

## 5.2 3-D Modeling

A quarter of modeled mandrel cross-section is depicted in Fig. 15. To investigate the distribution of the residual stresses at the inner surface of the workpiece in contact with the mandrel, the dimensions on the mandrel are normalized with respect to the total length of the shown section in the X direction. For the mandrel considered here, the dimensions L, L1, and L2 are 7.00 mm, 3.08 mm, and 4.62 mm, respectively. Accordingly, by considering point O as the origin of coordinates, normalized positions of the points O, A, B, E, C, D, and F in the X direction are given in the Table 6.

### *5.2.1 Residual stresses on the formed profile*

Figures 16 and 17 show the distributions of the three principal stresses and the Misses stress at the axial positions of 20 mm and 30 mm from one end of the tube, respectively. Also, the principal and equivalent strains at the axial position of 20 mm are plotted in Fig. 18. For the sake of comparison, the location of plots at the X direction (normalized direction) is shifted in Fig. 17 so that the normalized positions of the critical points could be the same in two axial positions. In Figs. 16, 17 and 18 symmetry of distributions around the center point E is observed. Points A and D have the largest stress magnitudes. These points at the edges of the groove are the first points of the inner surface that contact the mandrel and thus, are subjected to higher stresses and strain. The equivalent strain exceeds 0.75 in these regions while its value is less than 0.6 in other regions. Furthermore, the

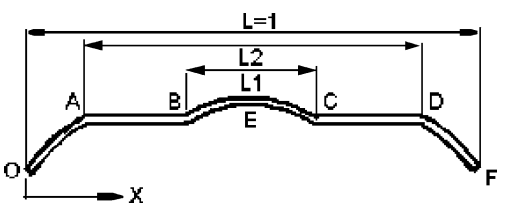


**Fig. 15** Quarter cross-section of mandrel used for producing internal helical grooves in tube

**Table 6** Relative normalized positions of the critical points on the produced profile

| Point | O | A | B | E | C | D | F |
|---|---|---|---|---|---|---|---|
| **Relative position** | 0.00 | 0.17 | 0.2 | 0.5 | 0.72 | 0.83 | 1.00 |

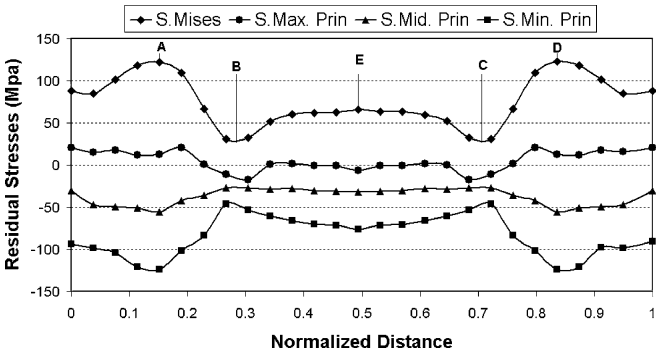


**Fig. 16** Distribution of principal and Mises residual stresses at a section 20 mm from one end of the tube

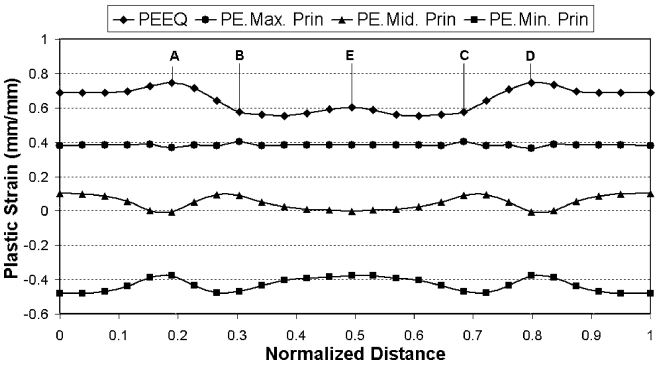


**Fig. 18** Distribution of principal and Mises residual stresses at the mid-section, 60 mm from one end of the tube

gradient of plastic strain is the largest at these points. Consequently, the residual stresses in these zones are more than other regions of inner surface of the workpiece.

Once contact in the AO and DF zones is occurred, point E is the first point of arc BEC (in Fig. 15) which contacts the inner surface of tube (profile) and so, plastic strains and residual stresses in this point are relatively higher than its adjacent regions. The last formed regions of the internal profile are points B and C and thus the strain and residual stresses at these points are the smallest. The maximum difference in distribution of Misses residual stress on inner surface is between points A and B and exceeds 95 MPa. From these results, it can be concluded that the residual stresses on the profiled inner surface of the produced tube strongly depend on the geometry and dimensions of the internal profile of the mandrel. Therefore, the inner edges of the grooves are the critical zones for residual stresses. It can also be observed that the by neglecting the internal profile in the simplified 2-D axisymmetric model of the process, inaccuracies in the prediction of residual stresses on the inner surface of the product are expected.

### *5.2.2 Pressure distribution on the mandrel*

The distribution of applied normal pressure on the profiled-mandrel section at the end of the hammers stroke, when this parameter has its extreme values, is given in Fig. 19 along the mandrel section. The highest pressure on the mandrel is observed at points A, D, and E where mandrel first contacts the workpiece and thus, the workpiece is under severe plastic deformation. Its amount exceeds 760 MPa at points A and D. At points B and C the applied pressure on the mandrel has its minimum value because these are the last points of contact. Therefore, outer edges of grooves are the critical regions where tool wear can occur quickly and should be controlled and optimized for tool life considerations.

The distribution of applied normal pressure on the mandrel's profile is given in Fig. 19 at four different axial positions 2 mm, 4 mm, 6 mm, and 8 mm away from the die land entrance. In this model, the length of the die land is 10 mm. it can be seen that the trend of pressure distribution are the same everywhere, but in general, the points further from the die land entrance have smaller pressures. With respect to the applied boundary conditions, the closer the

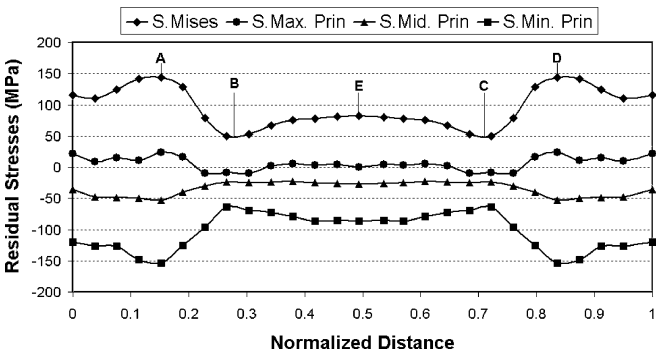


**Fig. 17** Distribution of principal and Mises residual stresses at a section 30 mm from one end of the tube

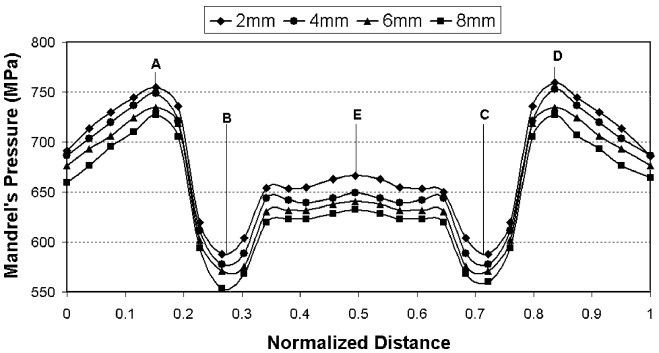


**Fig. 19** Distribution of normal pressure on the profiled surface of mandrel at the end of the hammers stroke

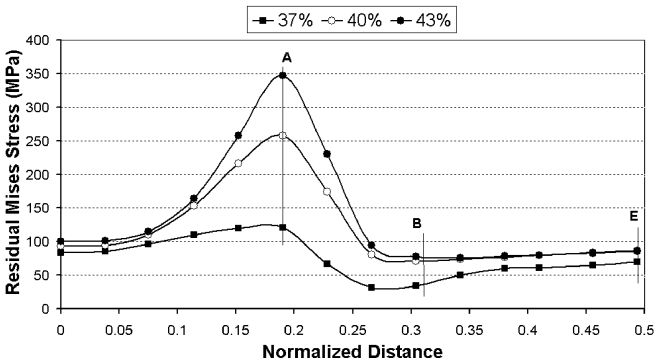


**Fig. 20** Distribution of the Mises residual stress on the profiled surface of tube for various tube area reductions

material is to the die inlet zone the easier is the axial flow of material, because it contacts hammers in a smaller region. Therefore, pressure at the end of the die land is less than pressure at its entrance.

### *5.2.3 Tube reduction*

To investigate the effects of reduction of tube cross-section on the residual stresses at the inner surface of the tube and on the mandrel pressure, the initial cross-section of the tube is held constant and the variation of area percent reduction is applied by varying the radial stroke of hammers. Since the profile OABECDF (in Fig. 15) is symmetric, only half of the profile (OABE) is modeled.

Residual stress distribution on the inner surface of the tube along the path of OABE profile for different percent reductions is depicted in Fig. 20. It can be observed that with increasing the tube reduction, residual stress increases significantly at zone A, while in other zones, especially in the BE zone, it varies only slightly. For better study of this effect, residual Misses stress variations at points A, B, and E are illustrated in Fig. 21. Increasing of area reduction from 37% to 46% causes stress increase of up to 350 MPa at zone A, while stresses at zones B and E only vary

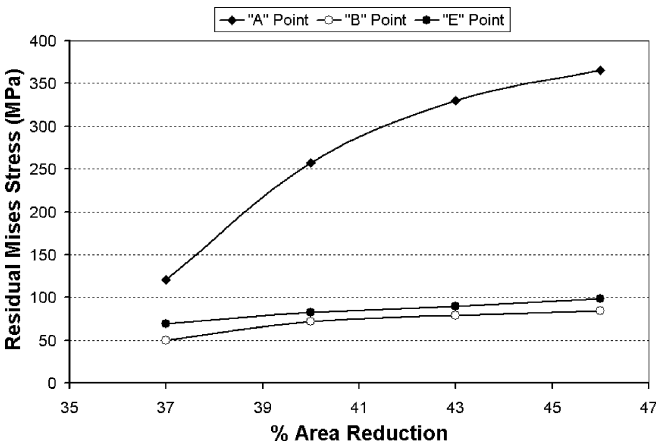


**Fig. 21** Variation of Mises residual stress vs. Tube area reduction at critical points of the groove profile

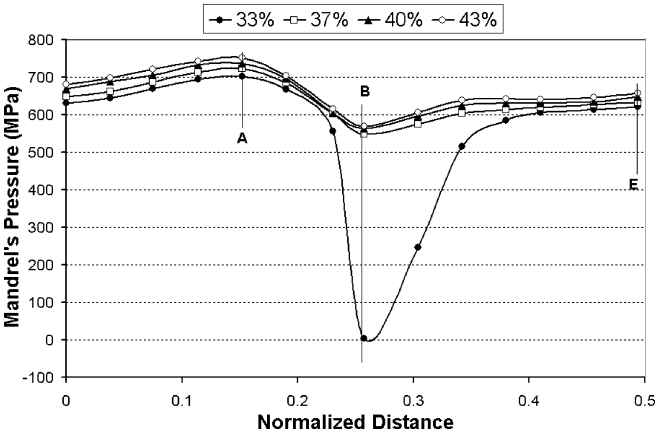


**Fig. 22** Distribution of normal pressure on the profiled surface of mandrel vs. tube area reduction

between 50 MPa and 100 MPa. Therefore, zone A is very sensitive to percent reduction of the cross section.

The pressure distribution on the mandrel along the OABE profile for several reduction levels is shown in Fig. 22. As mentioned previously, in all cases the highest and lowest pressures occur at point A and B, respectively. Contrary to the residual stresses, variations of pressure are almost uniform along the profile. The pressure rises with an increasing of reduction due to work hardening of material as well as larger sticking friction areas.

For 9% increase in reduction level, the pressure changes by 60 MPa, while this amount for the residual Misses stress at point A is 225 MPa. Therefore, percent reduction has less effect on pressure than on residual stress. Furthermore, there is no specific zone of profile with high sensitivity to the pressure. The only significant change in Fig. 22 is at point B when tube reduction reaches 33%, where it is seen that pressure is dropped to zero. This is because at this percent reduction, no contact between mandrel and work-piece occurs at point B. It means that this part of the cavity of the mandrel is not fully filled at this level of reduction. Consequently, if the cross-section reduction is less than a critical percentage, the desired profile may not be formed completely. Determination of this critical percentage is possible by surveying the residual stress at point B for various situations.

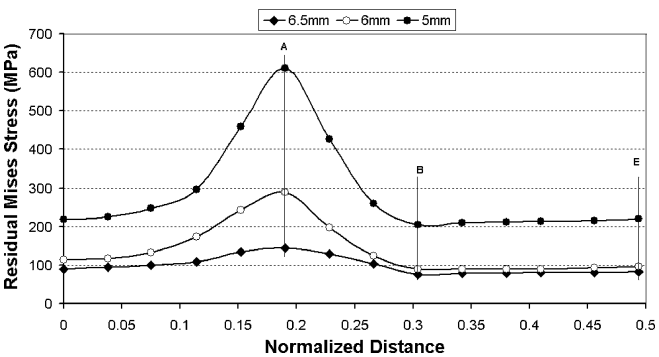


**Fig. 23** Distribution of the residual Mises stress on the profiled surface for various inner radii of the preform

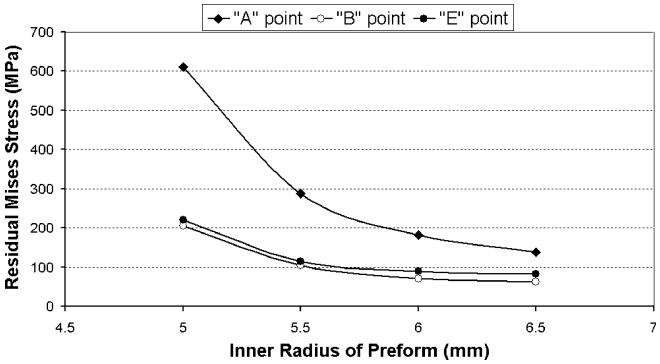


**Fig. 24** Variation of residual Mises stress with the inner radius of preform at critical positions on the section

### *5.2.4 Tube preform geometry*

In this section, the effects of preform geometry on the residual stress and pressure are studied. To investigate the effect of preform tube thickness, the outer radius of preform and final geometry of the forged tube are held constant and the simulation is run for inner radii of 5 mm, 5.5 mm, 6 mm, and 6.5 mm. Distribution of residual Misses stresses for various values of the inner radius of preform is shown in Fig. 23. It may be seen that the trends of residual stress variations are the same but stress values, particularly at point A, vary considerably for different inner radii. At the radius of 5 mm, stress at point A increases dramatically. For better study of this variation, residual Misses stress variations at points A, B, and E vs. the inner radius of the tube are illustrated in Fig. 24. Decreasing of the inner radius from 6.5 mm to 5 mm causes an increase of stress about 460 MPa at point A, while variations of stress at zones B and E are only 120 MPa. Therefore, zone A is particularly sensitive to the initial thickness of tube.

Distribution of normal pressure on the mandrel profile for several geometries of preform has been illustrated in Fig. 25. Variations of pressure at points A, B, and E are not the same and region A is the most sensitive to the variation of thickness. The graph in Fig. 26 shows that the variations of mandrel pressure are higher for larger inner radii.

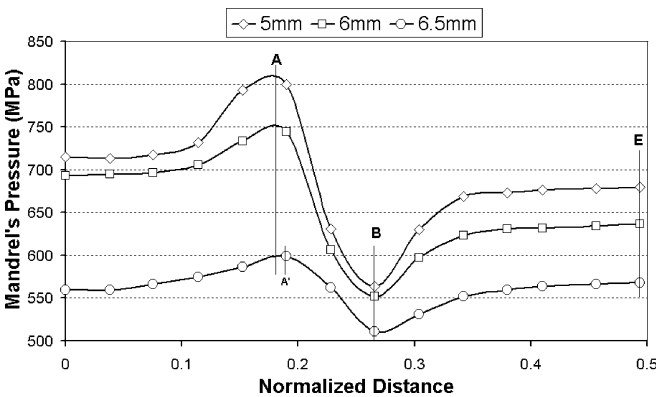


**Fig. 25** Distribution of normal pressure on the profiled surface of mandrel for various inner radii

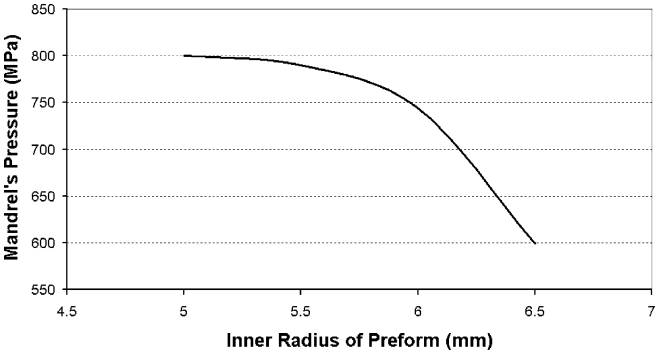


**Fig. 26** Variation of normal pressure at point A vs. the inner radius

### *5.2.5 Rotational feed*

An important process parameter that has not been investigated in previous studies is the rotational feed of the workpiece. This parameter cannot be modeled in axisymmetric studies. Because of using a 3-D model, the study of rotational motion is feasible here.

The rotation of workpiece and blowing of hammers are intermittent. So, rotational speed has been applied as the angle of rotation per blow with constant axial feed of workpiece. The frequency of blows and the axial feed of workpiece are selected as 800 stroke/min and 140 mm/min, respectively. Variations of the principal and the Misses residual stresses at the outer surface of the tube with respect to the rotational speed have been depicted in Fig. 27. It is seen in this figure that maximum and medium stresses vary only slightly, but the minimum stress decreases from −300 MPa to −200 MPa with a 30 rpm increase of rotational speed. Consequently, increasing of rotational speed causes a decrease of residual Misses stress at the outer surface of tube that contact with the hammers. This may result from the higher uniformity of deformation at higher rotational speed.

Variation of normal pressures on hammers and mandrel in the middle of die land position at the end of hammers stroke is shown in Fig. 28. The figure shows that the pressure on the mandrel drops slightly with an increase in rotational feed, while the pressure on the hammers shows a sharp increase. Consequently, while residual stresses on the produced tube and normal pressure on the mandrel may not

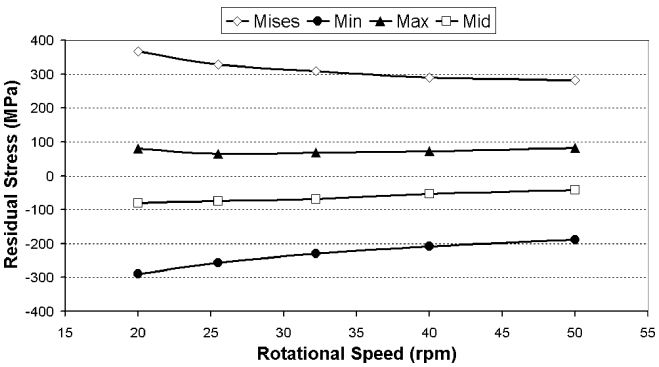


**Fig. 27** Distribution of stresses on the outer surface of the tube vs. rotational speed

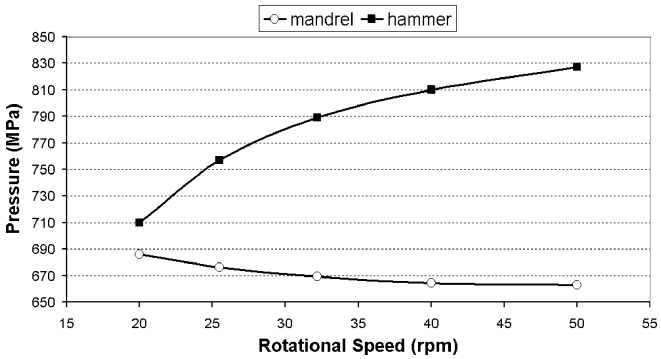


**Fig. 28** Variation of normal pressure on the mandrel and hammers vs. rotational speed

be a concern in this regard, but die pressure can be a limiting factor for increasing rotational feed.

## 6 Conclusion

In this work, a 3-D finite element model for simulation of radial forging of profiled tubes is developed and effects of parameters such as rotational feed and internal profile on residual stresses and pressure on the mandrel are studied. Furthermore, a validated axisymmetric finite element model is used to investigate other parameters such as axial feed per stroke, friction coefficient, die land length, die inlet angle, and preform thickness. The most important results of this work can be summarized as bellow:

- The axisymmetric developed model has good agreement with experiment.
- The factor that affects residual stresses the most is axial feed per stroke.
- Increasing friction, die land length, axial feed per stroke and thickness of preform causes an increase in die pressure and forging load, but the die inlet angle has a reverse effect.
- Residual stress distribution at the inner and outer surfaces in the axial direction of tube is uniform except at both ends of the tube.
- Residual stresses at the inner surface of the tube are significantly dependent on the geometry and dimension of mandrel profile. Therefore, neglecting the detailed geometry of internal profile leads to underestimating of maximum stresses.
- Inner edges of helical grooves on tube are the most critical zones for residual stresses. Theses stresses are very sensitive to the reduction and geometry of the preform. Also, residual stresses in these zones increase significantly with an increase of the percent reduction and decrease of inner radius of preform.
- The die pressure can be a restrictive factor for increase of rotational feed, while residual stresses and pressure on the mandrel take little effect from rotational feed.

The results obtained from these simulations provide a valuable insight into the parameters affecting radial forging process and provide an efficient tool for optimizing the design of forging die and mandrel. Further investigation of other parameters and experimental verification of 3-D results can strengthen these findings.

## References

1. Rauschnabel E, Schmidt V (1992) Modern application of radial forging and swaging in the automotive industry. J Mater Process Technol 35:371–383
2. Lahoti GD, Liuzzi L, Altan T (1977) Design of dies for radial forging of rods and tubes. J Mech Work Technol 1:99–109
3. Thompson EG, Hamzeh O, Jackman LA, Srivatsa SK (1992) A quasi-steady-state analysis for radial forging. J Mater Process Technol 34:1–8
4. Jang DY, Liou JH (1998) Study of stress development in axi-symmetric products produced by radial forging using a 3D nonlinear finite element method. J Mater Process Technol 74:74–82
5. Lahoti GD, Altan T (1976) Analysis of the radial forging process for manufacturing rods and tubes. J Eng Ind 98:265–271
6. Lahoti GD, Altan T, Dembowski PV (1976) Radial forging of tubes and rods with compound-angle dies. Fourth North America Metalworking Research Conference, Columbus, OH, May 1976, pp 87–93
7. Paukert R (1983) Investigation into metal flow in radial forging. Ann CIRP 32(1):211–214
8. Rodic T, Stok, Gologranc F, Owen DRJ (1987) Finite element modeling of a radial forging process. In: Lange K (ed) Adv Technol Plasticity 2:1065–1072
9. Domblesky JP, Jackman LA, Shivpuri R, Hendrick BB (1994) Prediction of grain size during multiple pass radial forging of alloy 718. In: Loria EA (ed) Superalloys 718, 625, 706 and various derivatives. TMS, Warrendale, PA, pp 263–272
10. Jackman A, Ramesh MS, Forbes-Jones R (1992) Development of a finite element model for radial forging of Superalloys, Proc Int. Symp. on the Metallurgy and Applications of superalloys, Pittsburgh, PA, TMS Sept 1992, pp 103–112
11. Domblesky JP, Shivpuri R, Mohamdein MK (1996) FEM simulation of multiple pass radial forging of pyromet, Proceeding of the Int. Symp. on the Metallurgy and Applications of superalloys, Pittsburg 26–29 June 1994
12. Domblesky JP, Shivpuri R, Painter B (1995) Application of the finite element method to the radial forging of large diameter tubes. J Mater Process Technol 49:57–74
13. Domblesky JP, Shivpuri R (1995) Development and validation of a finite element model for multiple-pass radial forging. J Mater Process Technol 55:432–441
14. Domblesky JP, Shivpuri R, Altan T (1994) A review of radial forging technology including preform design for process qptimization. AIAA Technical Library, Report No. AD-A278770, ARCCB-CR-94004
15. Subramanian TL, Venkateshwar R, Lahoti GDD, Lee FM (1979) Experimental and computer modeling of die cavity fill in radial forging of rifling. Process modeling- fundamentals and applications to metals. Proc Process Modeling Sessions, US, pp 185–203
16. ABAQUS (2005) Hibbit Karlson, Pawtucket, RI
17. Male AT, Cockroft MG (1964–65) A method for the determination of friction of metals under conditions of bulk plastic deformation. J Inst Met 93:38–45
18. Lee CH, Altan T (1972) Influence of flow stress and friction upon metal flow in upset of rings and cylinders. J Eng Ind ASME 7:75–82
19. Uhlig A (1965) deformation energy and tool forces in an idealized radial forging process. Metal 19:322 (in German)